Direct Aqueous Self-Assembly of an Amphiphilic Diblock Copolymer toward Multistimuli-Responsive Fluorescent Anisotropic Micelles

Gang Wu,[†,‡] Si-Chong Chen,[†] Chang-Lei Liu,[†] and Yu-Zhong Wang[*,†]

[†]Center for Degradable and Flame-Retardant Polymeric Materials (ERCEPM-MoE), National Engineering Laboratory of Eco-Friendly Polymeric Materials (Sichuan), State Key Laboratory of Polymer Materials Engineering, Sichuan University, Chengdu, Sichuan 610064, China and [‡]School of Energy Science and Engineering, University of Electronic Science and Technology of China, Chengdu, Sichuan 611731, China

ABSTRACT It is extremely important for emerging applications and still enormously challenging to develop multifunctional stimuli-responsive anisotropic polymeric micelles with integration of potentially targeted therapeutic and diagnostic function. Herein, we report a first example of fluorescent anisotropic micelles (FAMs) with Fe^{3+}, DTT, H_2O_2, and thermal responsive fluorescence and morphology. FAMs from direct aqueous self-assembly of amphiphilic diblock copolymer showed reversible "switch off/on" of aqua fluorescent emission and controllable structural change by sequential addition of Fe^{3+} and DTT. In addition, the FAMs had reversible dual-thermal responsiveness of fluorescence and morphology. This micelle could serve as a promising candidate for all-in-one application of quantitative detecting, imaging, drug delivery, and targeted release.

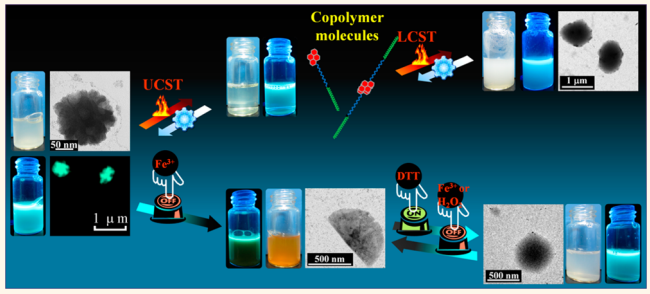

KEYWORDS: shape anisotropy · fluorescent · micelles · stimuli-responsive · block copolymers · self-assembly

Biological systems have evolved a number of fascinating anisotropic morphologies or structures to endow them with directionally dependent functions and properties. For instance, pollen grains have anisotropic patches on their surface, and heme and self-assembled aggregates of hydrophobin proteins show a Janus-like structure.[1] Inspired by nature, diversified synthetic anisotropic particles with asymmetric geometrical structures or heterogeneous chemical or physical compositions have been developed widely owning to their potential applications in biomedicine materials, display devices, solid stabilizers or surfactants, sensors, coatings, catalysis, building blocks for complex structures, *etc.*[2−9] Various bottom-up or top-down approaches have been implemented to construct anisotropic micro/nanoparticles so far.[10−19]

Comparing with relatively high-cost and complicated top-down methods,[20] the facile and controlled bottom-up approaches involving employment and manipulation of molecules or particles, which represent persistent research motivation of current materials science, are more elegant for fabricating a multitude of anisotropic particles based on soft matter in bulk, solution, or thin films.[21−28] Typically, aqueous self-assembly of amphiphilic block copolymers has emerged as a versatile technique to create micro/nano core−shell particles with a non-centrosymmetric shape and component distribution within the core and/or on the shell surface, such as patchy micelles,[29] patchy nanocapsules,[30] multicompartment micelles,[31−34] and others.[35−38] Non-centrosymmetric anisotropic micelles have introduced an opportunity for the solution of some challenges in biomedical applications. Like nonspherical nanostructures, the blood circulation time was prolonged,[39] and cellular uptake was increased.[40] In addition, the patches on the shell surface could provide specific sites for cell binding, and the compartments in the core can support

* Address correspondence to yzwang@scu.edu.cn.

Received for review March 3, 2015 and accepted April 10, 2015.

Published online April 10, 2015
10.1021/acsnano.5b01370

multiple/selective loading, transport, and release of various therapic or diagnostic compounds.[35,41] Even though considerable success in the design and preparation of anisotropic micelles with a single function has been achieved, developing multifunctional stimuli-responsive anisotropic micelles for emerging applications, especially smart "theranostics", which integrates a targeted therapeutic and diagnostic function within a single drug delivery system, presents a serious challenge and is still in its infancy.[42−45]

Herein, we report a novel micelle with bright fluorescent emission and anisotropic structure from direct aqueous self-assembly of an amphiphilic diblock copolymer. This fluorescent anisotropic micelle (FAM) showed a "switch off" of fluorescence and change of morphology exclusively relating to Fe^{3+}. Moreover, the addition of DL-dithiothreitol (DTT) can switch on the fluorescence and result in the formation of new nanoparticles. By sequential addition of DTT and Fe^{3+}, the "switch on/off" of fluorescence and transition of morphology can be reversibly repeated. In addition, the FAMs were dual thermally responsive, corresponding to an upper critical solution temperature (UCST) and a lower critical solution temperature (LCST), which leads to a reversible change of fluorescence and morphology. This is the first example of anisotropic micelles with a two-in-one feature of fluorescence change and morphological transition by applying multiple stimuli.

RESULTS AND DISCUSSION

The FAMs were constructed from a pyrene-functionalized amphiphilic copolymer building block in water. The amphiphilic copolymer denominated Py-$PPDO_7$-*b*-PEG_{16} was prepared by a three-step strategy including ring-opening polymerization, carboxylation, and coupling reaction (Figure S1). As shown in Scheme 1, the copolymer contains three vital parts: a poly(*p*-dioxanone) (PPDO) chain with an average of seven *p*-dioxanone units as a hydrophobic, crystalline, and thermally responsive segment, a poly(ethylene glycol) monomethyl ether (MPEG) chain with an average of 16 ethylene glycol units as a hydrophilic and thermally responsive segment, and a pyrene moiety attached at the chain end as a fluorophore and a binding site of Fe^{3+}. The self-assembly of this amphiphilic copolymer in water can result in nanoparticles with anisotropic structure according to our previous research,[46−50] and the nanoparticles will be fluorescent due to incorporation of the pyrene group. Importantly, the addition of Fe^{3+} can induce a morphological change of FAMs accompanied by a "switch off" of fluorescence due to damage of pyrene $\pi-\pi$ stacking and potential interaction of Fe^{3+}-pyrene,[51,52] revealing Fe^{3+} responsiveness. Subsequently, by DTT-induced reduction of Fe^{3+} to Fe^{2+}, the fluorescence is switched on, and new particles are formed. The "switch off" of fluorescence and the structure recovery of particles can be achieved

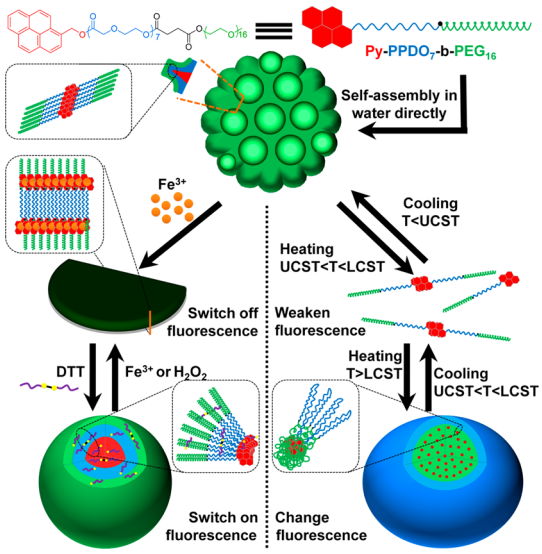

Scheme 1. Schematic representation of the self-assembly of Py-$PPDO_7$-b-PEG_{16} and the multistimuli-responsive fluorescence and morphology of FAMs.

by addition of fresh Fe^{3+} or H_2O_2-induced oxidation of Fe^{2+} to Fe^{3+}. In addition, transition of FAMs to copolymeric molecules to giant ellipsoidal particles accompanied by a change of fluorescence intensity is achieved reversibly by increasing or decreasing the temperature, indicating a dual thermal responsiveness.

FAMs were obtained by directly adding the copolymer into water, annealing at 90 °C, and aging at 25 °C. At room temperature, the white aqueous suspension of FAMs was quite stable and emitted intense aqua fluorescence when exposed to 365 nm UV light (Figure 1a). However, FAMs were molecularly soluble in $CHCl_3$, and pyrene moieties were chiefly in the form of a ground-state monomer, supported by intense blue fluorescence and the corresponding emission spectrum of the $CHCl_3$ solution of Py-$PPDO_7$-*b*-PEG_{16} (Figures S4 and S5). According to the features of pyrene and the amphiphilic molecule, the aqua emission of the suspension was assigned to the fluorescence of the pyrene excimer generated by a spontaneous aggregation of this amphiphilic copolymer in water, which promoted the $\pi-\pi$ stacking of pyrene moieties.[53] FAMs were characterized by confocal laser scanning microscopy (CLSM), transmission electron microscopy (TEM), and atomic force microscopy (AFM). CLSM showed that FAMs were fluorescent in a aqua region of the spectrum (Figure 1b), and their profile was undulate (Figure 1c). TEM further confirmed the undulate profile of FAMs and described in more detail their patchy structure with some cells of about 25 nm on the surface (Figure 1d−f), which was supported by AFM images (Figure 1g−i). The mean diameters of FAMs from TEM and AFM images were 167 ± 61 and 203 ± 51 nm (Figure 1j), approaching the $\langle D_h \rangle$ of 228 nm determined by dynamic light scattering (DLS) (Figure 1k). In addition, the critical micelle concentration

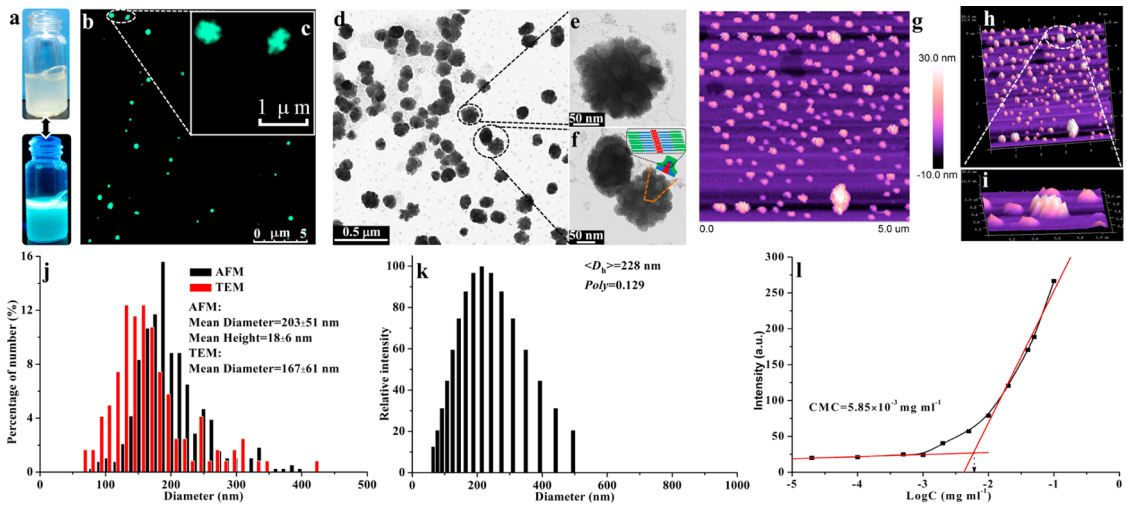

Figure 1. (a) Photographs of a formed aqueous suspension of FAMs under visible or UV (365 nm) light. (b and c) CLSM images of FAMs in water. (d, e, and f) TEM images of dry FAMs under different magnifications. (g, h, and i) AFM 2D and 3D height images of dry FAMs. (j) Statistic diameter distribution of dry FAMs from AFM and TEM images. (k) Diameter distribution, intensity-averaged hydrodynamic diameter ($\langle D_h \rangle$), and polydispersion (*Poly*) of FAMs in water from DLS. (l) Determination of critical micellization concentration (CMC) from the fluorescence intensity of Nile Red in a copolymeric aqueous solution at 621 nm *versus* logarithm concentrations of copolymer at 25 °C.

(CMC) of FAMs obtained from fluorescent measurement by using Nile Red as a fluorescent probe was 5.85×10^{-3} mg mL^{-1} (Figure 1l), indicating the facile micellization and a potentially good stability of micelles as applied to a drug-controlled-release carrier in the bloodstream.[54]

The pyrene-excimer-based fluorescent sensors for various analytes (*e.g.*, ions,[55] small molecules,[56] nucleic acids,[57,58] or proteins[59]) have been reported widely due to high quantum yield and longer lifetime.[53] Herein, as Fe^{3+} was added at room temperature, the white suspension of FAMs changed to yellow, and the aqua fluorescence was switched off (Figure 2a). Fluorescent emission measurements showed two types of emission peaks (350−450 and 450−550 nm) assigned to the pyrene monomer (PM) and pyrene excimer (PE), respectively, and the emission spectra were weakened steadily with the increase of [Fe^{3+}] (Figure 2b). Relative fluorescence intensity (I/I_0) decreased with the increase of [Fe^{3+}] (Figure 2c). Detection limits (DLs) defined as the concentration of analyte where fluorescence was weakened or enhanced by 10% were determined to be 22.3 and 80.4 μM for PM and PE, respectively. The DL is quite comparable to that of prior methods (*e.g.*, flame atomic absorption spectrometry, ion-selective electrodes, and UV−vis spectrometry), and the fluorescence cannot be quenched effectively by other various valence metal ions (Figure 2h), indicating a potential prospect as a "switch off" fluorescence probe for selective detection of Fe^{3+} in an aqueous environment. Notably, a wide red shift of excimer signal from 481 to 495 nm occurred, reflecting the presence of interactions between pyrene and Fe^{3+}. We infer that the "switch off" of aqua fluorescence could be attributed to a specific complexation of Fe^{3+} and polycyclic aromatic pyrene accompanying the disruption of $\pi-\pi$ stacking of pyrene moieties, similar to the gas-phase cation complexes of iron and pyrene.[51,52] Indeed, the plots of $1/(I_0 - I)$ *versus* 1/[Fe^{3+}] in terms of the Benesi−Hildebrand method, which was widely used to study stoichiometric complexation *via* a nonbonding interaction, showed a good linear fit (Figure S6),[60,61] solidly confirming the formation of a 1:1 complex of PE or PM with Fe^{3+}. The binding or association constants (K) for PE and PM were also estimated to be 1.384×10^3 and 4.560×10^3 M^{-1}, respectively.

Glutathione (GSH) as a tripeptide biothiol exists widely in the eukaryotic cytosol with a high intracellular concentration (approximately 1−10 mM) and low extracellular concentration (approximately 2−20 μM).[62,63] GSH serves a critical role in maintaining the redox state of the cell,[64] and the imbalance of reduced and oxidized GSH (GSH/GSSG) is directly linked to various diseases such as cancer and Alzheimer's disease.[65] In comparison with GSH, DTT exhibits a similar redox behavior and often is selected to mimic an intracellular GSH reductive environment.[66−68] Herein, when DTT was added into the above yellow suspension, the aqua fluorescence was switched on and a white suspension was regenerated (Figure 2a). Moreover, on increasing the amount of DTT, the emission spectra were enhanced gradually, and a broad blue shift of excimer signal from 498 to 481 nm was observed (Figure 2d). A quantitative relation between I/I_0 and [DTT] is shown in Figure 2e. It can be found that the I/I_0 of PM and PE increased with the increase of [DTT] and tended to be stable at about 50 mM. The DLs of PM and PE were 0.2824 and 0.2903 mM, respectively, implying that an available detecting concentration of DTT is above the

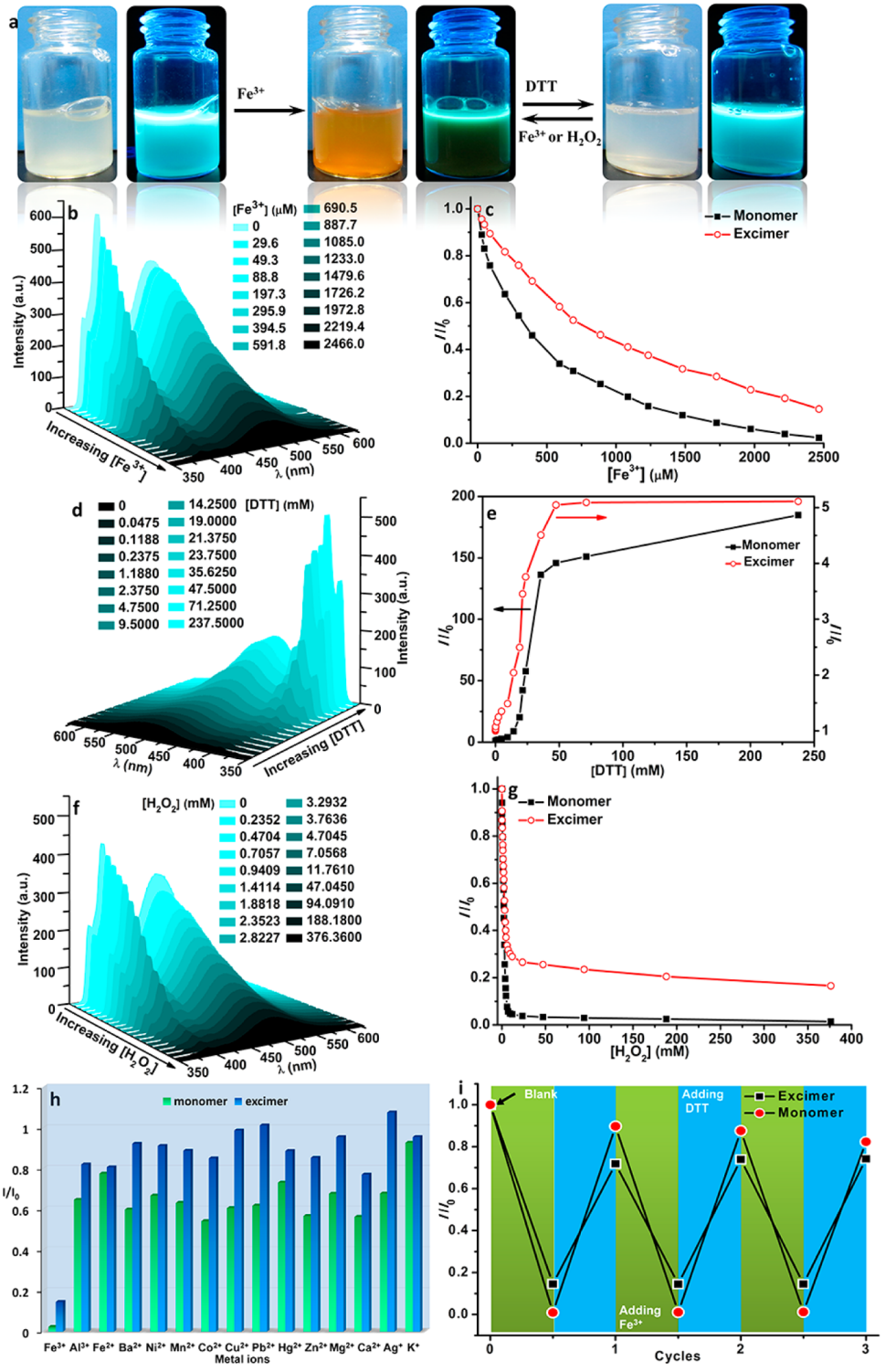

Figure 2. (a) Photographs with different additives under visible and UV (365 nm) light. (b, d, and f) Fluorescence emission spectra with different [Fe^{3+}], [DTT] (after 12 h of adding 2 equiv of Fe^{3+} relative to pyrene moieties), and [H_2O_2] (after 12 h of adding 1 equiv of DTT relative to Fe^{3+}), respectively. (c, e, and g) Relevant plots of I/I_0 *versus* [Fe^{3+}], [DTT], and [H_2O_2], respectively. (h) Column chart of I/I_0 with different metal ions. (i) I/I_0 upon sequential addition of 2 equiv of Fe^{3+} and DTT relative to pyrene moieties. I and I_0 represent fluorescence intensity with and without analytes, respectively.

extracellular but below the intracellular GSH concentration. Thus, the copolymer could be used as a fluorescent probe for intracellular GSH without interference from extracellular GSH. Because DTT or GSH can reduce Fe from high valence to low valence,[69,70] and the addition of 2 equiv of Fe^{2+} caused only a quite limited reduction of the fluorescent emission (Figure S7), the reason for the "switch on" of aqua fluorescence could be attributed to a dissociation of pyrene/Fe^{3+} complexes induced by a reduction of Fe^{3+} to Fe^{2+} in the

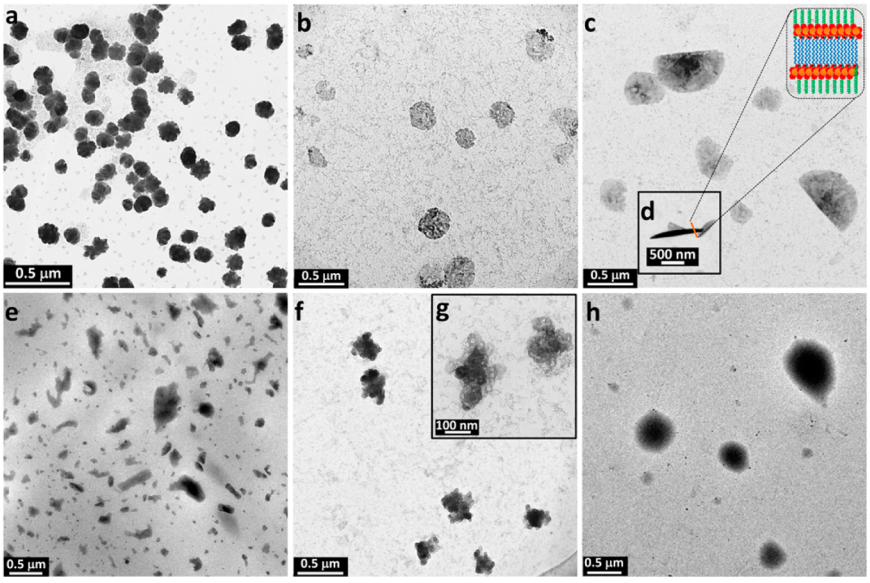

Figure 3. TEM images of FAMs at different times after adding different analytes at 25 °C: without analytes (a); addition of Fe^{3+} (2 equiv relative to pyrene moieties), (b) 2 h, (c and d) 24 h; addition of DTT after the addition of Fe^{3+} (2 equiv relative to Fe^{3+}), (e) 5 min, (f and g) 1.5 h, (h) 24 h.

presence of DTT and then the reconstruction of $\pi-\pi$ stacking of pyrene moieties by reassembly of copolymer for establishing a new hydrophilic−hydrophobic balance. Importantly, when adding fresh Fe^{3+} or H_2O_2 into the regenerated suspension, the aqua fluorescence was switched off again (Figure 2a). The cycle of switching on and off of fluorescent emission can be reversibly repeated multiple times by the sequential addition of DTT and Fe^{3+} (Figure 2i). However, it is predictable that the repeated switching is not sustainable due to the possible swelling capability of DTT and its oxidized products for the copolymer and potential hydrolytic degradation of PPDO. For the addition of H_2O_2, an obvious oxidation of Fe^{2+} to Fe^{3+} occurred. The emission spectra were weakened steadily with the increase of $[H_2O_2]$, and a red shift of the excimer signal from 481 to 492 nm was also observed (Figure 2f). I/I_0 decreased sharply with an increase of $[H_2O_2]$ and tended to be stable at about 10 mM (Figure 2g). The DLs of PE and PM were 0.1362 and 0.2246 mM, separately.

Upon addition of Fe^{3+} to the aqueous suspension at 25 °C, due to the change of the hydrophilic−hydrophobic balance, the FAMs were disassembled gradually and disrupted into small fragments within 2 h (Figure 3b). With prolonging time, a new hydrophilic−hydrophobic balance was established, and molecular rearrangement promoted small fragments to reassociate into nanosheets with an irregular shape (Figure S9). After 24 h, semicircular nanosheets (SNSs) with the largest radius of 580 nm and a 120 nm maximum thickness were obtained (Figure S10, Figure 3c and d). The formation mechanism of SNSs is not very clear. However, the pyrene-Fe^{3+} complex as a more hydrophilic polymeric head than pyrene is in favor of this planar structure (Figure 3c, inset), and an asynchronous association similar to asynchronous contraction, which induced the formation of sheet-like superstructures, should also contribute to produce SNSs.[71] Moreover, on adding DTT to the above system, the SNSs were disrupted gradually (Figure 3e). This is a result of the DTT-induced reduction of Fe^{3+} to Fe^{2+}. In that way, hydrophobic pyrene as a polymeric head was restored, and the hydrophilic−hydrophobic balance was disrupted. Afterward, a new hydrophilic−hydrophobic balance was established gradually by copolymer reassembly. It was found in Figure 3f and g that the new nanoparticles were formed after 1.5 h of adding DTT, and their inner structure was like multicompartment micelles. Owing to the swollen possibility of copolymer chains, adding DTT and oxidized products of DTT could promote the formation of this structure, similar to the role of organic diamines.[35] The further swelling led to the production of spherical particles after 24 h (Figure 3h). Hence, the SNSs with DTT-controlled structural change behavior are expected to be employed as targeted-release vehicles encapsulating anticancer drugs in tumor tissues.

Our previous research reveals that PPDO-based amphiphilic copolymers in water show thermal responsiveness.[72] Herein, with increasing temperature, the white suspension of FAMs gradually underwent two types of phase transition, namely, turbid-to-transparent and transparent-to-turbid, corresponding to UCST and LCST, respectively (Figure 4a). UCST and LCST in the heating stage were obtained by variable-temperature turbidity measurements (Figure 4b), *i.e.*, 48.2 and 67.8 °C. The thermal responsiveness was hysteretic in the cooling stage, especially UCST-type phase transition. Importantly, the aqua fluorescence turned to

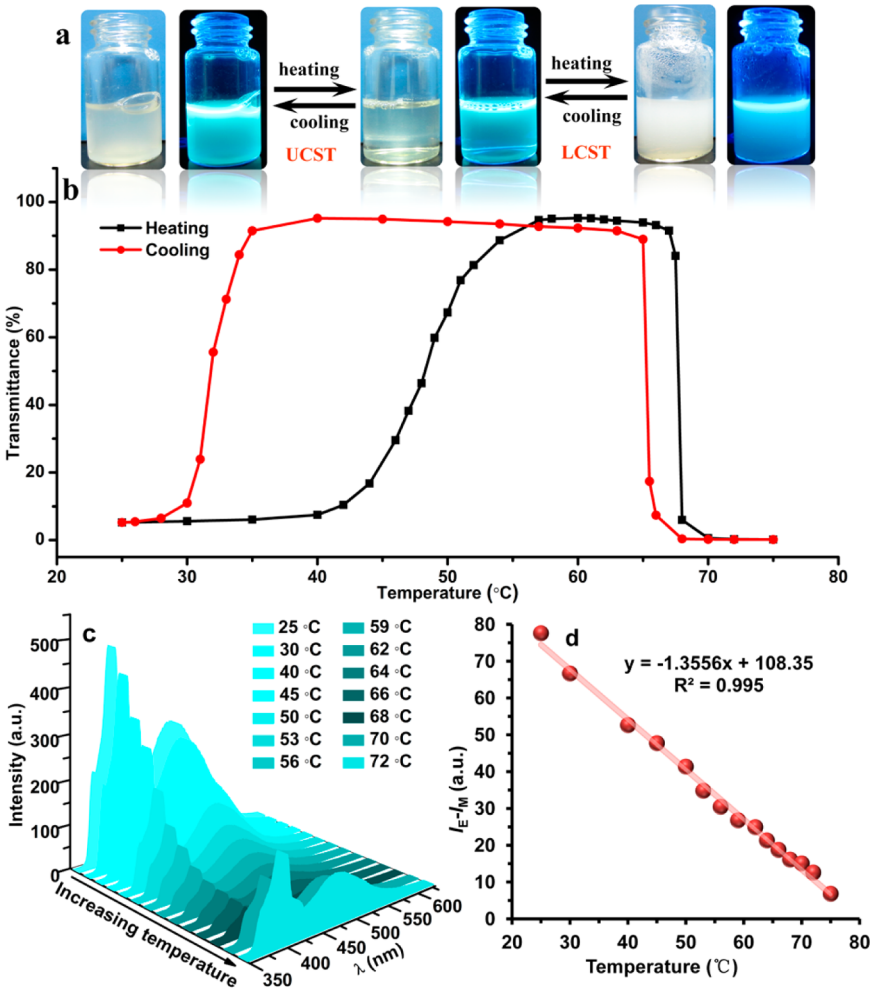

Figure 4. (a) Photographs of FAMs in water at different temperatures under visible or UV (365 nm) light. (b) Transmittance *versus* temperature curves with a heating/cooling cycle. (c) Fluorescence emission spectra at different heating temperatures. (d) Difference of fluorescence intensity ($I_E - I_M$) as a function of heating temperature (light red line is a linear fitted curve of points). I_E and I_M correspond to fluorescence intensity of the excimer around 481 nm and the monomer around 377 nm, respectively.

bluish-green as the temperature increased to above the LCST (Figure 4a). The emission spectra were weakened gradually at first and then enhanced on increasing the temperature from 25 to 72 °C (Figure 4c). A detailed analysis showed that the difference of fluorescence intensity ($I_E - I_M$) was linearly temperature-dependent (Figure 4d), indicating that FAMs could act as a fluorescent thermometer. According to the results of variable-temperature ^{1}H NMR (VT-^{1}HNMR), the mechanism of phase transition and fluorescence change should be the conversion of the hydrophilic–hydrophobic property of PPDO and PEG chains with increasing temperature (Figure S11), which alters the association state of copolymer molecules and the pyrene head.

In addition, a stepwise structural change of FAMs was clearly observed by TEM during the heating and cooling process. On increasing the temperature to 60 °C between the UCST and LCST, a few spherical particles were observed instead of FAMs (Figure 5b), indicating that a thermal-conducted disassembly had occurred. The studies of VT-^{1}HNMR and NANO DSC suggested that the reasons for this result could be dissolution and melting of semicrystalline PPDO located in hydrophobic regions as well as a change of the hydrophilic–hydrophobic balance (Figures S11 and S12).[46,72] This structural change probably has potential applications in the targeted release of encapsulated anticancer drugs by hyperthermia therapy in tumor tissues. On further elevating the temperature to 75 °C above the LCST, a number of ellipsoidal particles (EPs) with an approximately 1 μm average major axis and approximately 750 nm average minor axis were observed (Figure 5c), revealing a reassembly of copolymeric molecules driven by the change of the hydrophilic–hydrophobic balance due to a dehydration of PEG chains at higher temperature.[73] This mechanism of reassembly was supported by VT-^{1}HNMR (Figure S11). As the system was gradually cooled to room temperature, EPs disassembled first (Figure 5d),

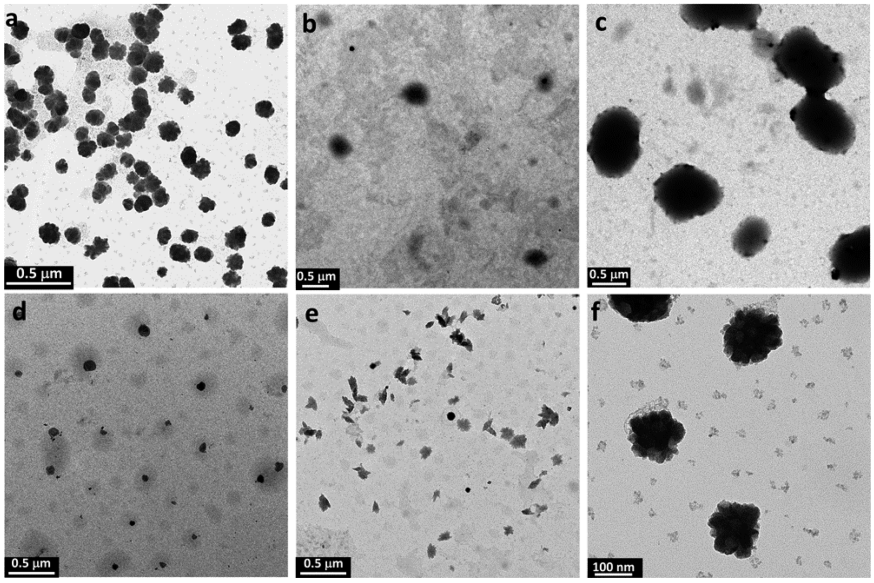

Figure 5. TEM images of FAMs at different temperatures: heating process, (a) 25 °C, (b) 60 °C, and (c) 75 °C; cooling process, (d) 65 °C, (e) 45 °C, and (f) 25 °C.

and then copolymers self-assembled again and regenerated FAMs (Figure 5e and f). This process was also monitored by VT-^{1}HNMR (Figure S11). The results were reversed compared with those of the heating process, reflecting a reversible mechanism for the formation and thermal-conducted structural change of FAMs.

CONCLUSION

In summary, we have presented a novel class of polymeric micelles with fluorescence and anisotropic structure, *i.e.*, FAMs, that exhibit multiple-stimuli (*e.g.*, Fe^{3+}, thermal, DTT, H_2O_2)-responsive fluorescence and morphology through the direct aqueous self-assembly of the amphiphilic diblock copolymer Py-PPDO$_7$-*b*-PEG$_{16}$. During addition of Fe^{3+}, the morphological change of FAMs to semicircular nanosheets was accompanied by a "switch off" of fluorescence as a result of the specific complexation of Fe^{3+} and pyrene. Subsequently, by adding DTT, the fluorescence was switched on, and the nanosheets were transformed to spherical nanoparticles. The on−off switchable fluorescence and morphological transition can be reversibly repeated multiple times *via* sequentially adding DTT and Fe^{3+}. In addition, the dual thermal-controllable fluorescent property and structural change of FAMs corresponding to the UCST and LCST were achieved reversibly. Accordingly, we believe that FAMs could be a promising candidate for an all-in-one function of detecting and imaging physiologically relevant factors and bioactive molecules (*e.g.*, temperature, Fe^{3+}, or disulfide) as well as drug delivery and targeted release. The development of biomedical applications is currently under way.

EXPERIMENTAL SECTION

Materials. 1-Pyrenemethanol was purchased from Alfa Aesar. PDO (99.9%) with a melting point of 25 °C was provided by the Pilot Plant of the Center for Degradable and Flame-Retardant Polymeric Materials (Chengdu, China), dried over CaH_2 for 48 h, and then distilled under a reduced pressure of 70 Pa just before use. Poly(ethylene glycol) monomethyl ether (degree of polymerization = 16, M_n = 0.750 kDa) was purchased from Sigma-Aldrich. Stannous octoate ($SnOct_2$) (95%) was purchased from Sigma-Aldrich and was stored in glass ampules under argon after being diluted with anhydrous toluene. Nile Red (analytical grade) was purchased from Sigma-Aldrich. *N*,*N*′-Dicyclohexylcarbodiimide (DCC) (99%) was purchased from Sinopharm Chemical Reagent Co. Ltd. (Shanghai, China). 4-(Dimethylamino)pyridine (DMAP, 99%) and succinic anhydride (SA, 99%) were used as purchased from Nanjin Tianhua Reagent Co. Ltd. (Jiangsu, China) and Bodi Chemical Factory (Tianjin, China), respectively. DL-Dithiothreitol was purchased from Wolsen Biotechnology Co. Ltd. (Xi'an, China) and used as received. $FeCl_3$ was purchased from Sinopharm Chemical Reagent Co. Ltd. (Shanghai, China) and used as received. Other reagents of AR grade were purchased from Bodi Chemical Factory and used after further purification as follows: triethylamine (TEA) was dried over CaH_2 for 48 h and distilled just before use; dioxane and toluene were dried by refluxing over Na/benzophenone complex and distilled just before use; $CHCl_3$ was washed three times by distilled water, dried by refluxing over P_2O_5, and distilled just before use.

Synthesis of Py-PPDO-OH. Under an Ar atmosphere, anhydrous PDO (1.020 g, 10.00 mmol) and 1-pyrenemethanol (0.580 g, 2.50 mmol) were charged into a rigorously dried 10 mL flask, which was degassed at 50−55 °C in a vacuum line for 2 h, purging three times with dry nitrogen. After the solution temperature was increased to 80 °C, a 0.2 M $SnOct_2$ toluene solution (0.1 mL) as a catalyst was injected, and the reaction was allowed to proceed for 48 h at 80 °C. The reactors were cooled rapidly to room temperature. The crude product was dissolved in $CHCl_3$ and then precipitated in anhydrous ethyl ether. After the precipitate was filtered, the products were dried at 40 °C under vacuum until constant weight. The Py-PPDO-OH sample was obtained in 91.3% yield with Dp =7, $M_{n,NMR}$ = 0.946 kDa,

$M_{n,GPC}$ = 0.990 kDa, and M_w/M_n = 1.48. ^{1}H NMR (400 MHz, $CDCl_3$, δ): 8.02−8.29 (m, 1H, CHC*H*C or CHC*H*CH), 5.93 (s, 2H, CCH_2O), 4.34 (m, 2H, CH_2CH_2OC(=O)), 4.16 (s, 2H, OC(=O)CH_2O), 4.07 (s, 2H, CCH_2OC(=O)CH_2O), 3.78 (s, 2H, CH_2CH_2OC(=O)), 3.65−3.75 (m, 2H, OCH_2CH_2OH), 3.65−3.75 (m, 2H, OCH_2CH_2OH). The ^{1}H NMR spectrum and GPC curve of the Py-PPDO-OH are shown in Figure S2 and Figure S3, respectively.

The degree of polymerization (Dp) of Py-PPDO-OH was calculated by ^{1}H NMR:

$$\mathrm{Dp} = \frac{A_{4.05\ -\ 4.25\mathrm{ppm}}}{A_{5.93\mathrm{ppm}}} \quad (1)$$

where $A_{4.05-4.25\ \ ppm}$ and $A_{5.93\ \ ppm}$ are the integrals at 4.05−4.25 and 5.93 ppm, respectively.

The $M_{n,NMR}$ of Py-PPDO-OH was calculated by ^{1}H NMR as follows:

$$M_{n,\,NMR} = 102 \times \mathrm{Dp} + 232 \quad (2)$$

Synthesis of MPEG-COOH. First, MPEG (10.000 g, 13.33 mmol) was charged into a rigorously dried 100 mL flask. After the flask was dried at 60 °C in a vacuum for 6 h and filled with Ar, 40 mL of anhydrous dioxane was injected using a syringe to dissolve the MPEG. When the system became homogeneous, a 10 mL anhydrous dioxane solution of succinic anhydride (1.467 g, 14.66 mmol) and DMAP (0.895 g, 7.33 mmol) was injected into the flask *via* a syringe under an Ar atmosphere. Meanwhile anhydrous TEA (2 mL) was charged into the flask *via* a syringe, and the reaction was allowed to proceed for 24 h at 25 °C under an Ar atmosphere. The crude product was precipitated in anhydrous ethyl ether. Then the precipitate was filtered, washed, and dried. Finally, the MPEG-COOH was obtained in 89.5% yield with a Dp = 16, $M_{n,NMR}$ = 0.836 kDa, $M_{n,GPC}$ = 0.952 kDa, and M_w/M_n = 1.11. ^{1}H NMR (400 MHz, $CDCl_3$, δ): 4.25 (t, 2H, CH_2C(=O)OCH_2CH_2), 3.65 (s, 4H, OCH_2CH_2O), 3.38 (s, 3H, $CH_2CH_2OCH_3$), 2.65 (m, 4H, C(=O)CH_2CH_2COOH). The ^{1}H NMR spectrum and GPC curve of the MPEG-COOH are shown in Figure S2 and Figure S3, respectively.

The Dp of MPEG-COOH was calculated by ^{1}H NMR using eq 3.

$$\mathrm{Dp} = \frac{3 \times A_{3.65\mathrm{ppm}}}{2 \times A_{3.38\mathrm{ppm}}} + 1 \quad (3)$$

where $A_{3.65\ \ ppm}$ and $A_{3.38\ \ ppm}$ are the integrals at 3.65 and 3.38 ppm, respectively.

The $M_{n,NMR}$ of MPEG-COOH was calculated by ^{1}H NMR as follows:

$$M_{n,\,NMR} = 44 \times \mathrm{Dp} + 32 + 100 \quad (4)$$

Synthesis of Py-PPDO-*b*-PEG Copolymer. The Py-PPDO-*b*-PEG copolymer was synthesized by coupling using DCC as coupling agent. First, dry MPEG-COOH (1.000 g, 1.20 mmol) with Dp = 16 and Py-PPDO-OH (0.957 g, 1.01 mmol) with Dp = 7 were charged into a rigorously dried 10 mL flask. After the flask was degassed in a vacuum line and filled with Ar, repeating three times, 4 mL of anhydrous $CHCl_3$ was injected into the flask *via* a syringe under an Ar atmosphere. Since the compounds were dissolved completely, 1 mL of an anhydrous $CHCl_3$ solution of DCC (0.291 g, 1.41 mmol) and DMAP (0.034 g, 0.28 mmol) was injected. The coupling reaction was carried out for 24 h at 25 °C under an Ar atmosphere. The reaction mixture was filtered, precipitated in anhydrous ethyl ether, filtered, washed with anhydrous ethyl ether, and dried at 40 °C under vacuum until constant weight in sequence. Finally, the Py-PPDO-*b*-PEG copolymer was obtained in 81.3% yield with a $Dp_{(Py\text{-}PPDO)}$ = 7, $Dp_{(MPEG)}$ = 16, $M_{n,NMR(copolymer)}$ = 1.764 kDa, $M_{n,GPC(copolymer)}$ = 2.017 kDa, and M_w/M_n = 1.13. ^{1}H NMR (400 MHz, $CDCl_3$, δ): 8.02−8.29 (m, 1H, CHC*H*C or CHC*H*CH), 5.93 (s, 2H, CCH_2O), 4.33 (m, 2H, CH_2CH_2OC(=O)), 4.30 (t, 2H, OCH_2CH_2OC(=O)), 4.24 (t, 2H, CH_2C(=O)OCH_2CH_2), 4.17 (s, 2H, OC(=O)CH_2O), 4.07 (s, 2H, CCH_2OC(=O)CH_2O), 3.78 (s, 2H, CH_2CH_2OC(=O)), 3.64 (s, 4H, OCH_2CH_2O), 3.37 (s, 3H, $CH_2CH_2OCH_3$), 2.65 (s, 4H, C(=O)CH_2CH_2COOCH_2). The ^{1}H NMR spectrum and GPC curve of the Py-PPDO-*b*-PEG copolymer are shown in Figure S2 and Figure S3, respectively.

The Dp of the PPDO block ($Dp_{(Py\text{-}PPDO)}$) in the Py-PPDO-*b*-PEG copolymer was calculated by ^{1}H NMR:

$$\mathrm{Dp}_{(Py\text{-}PPDO)} = \frac{A_{4.05\ -\ 4.25\mathrm{ppm}}}{A_{5.93\mathrm{ppm}}} \quad (5)$$

where $A_{4.05-4.25\ \ ppm}$ and $A_{5.93\ \ ppm}$ are the integrals at 4.05−4.25 and 5.93 ppm, respectively.

The Dp of the MPEG block ($Dp_{(MPEG)}$) in the Py-PPDO-*b*-PEG copolymer was calculated by ^{1}H NMR:

$$\mathrm{Dp}_{(MPEG)} = \frac{3 \times A_{3.64\mathrm{ppm}}}{2 \times A_{3.37\mathrm{ppm}}} + 1 \quad (6)$$

where $A_{3.64\ \ ppm}$ and $A_{3.37\ \ ppm}$ are the integrals at 3.64 and 3.37 ppm, respectively.

The $M_{n,NMR}$ of the Py-PPDO-*b*-PEG copolymer ($M_{n,NMR(copolymer)}$) was calculated by ^{1}H NMR as follows:

$$\begin{aligned} M_{n,\,NMR(copolymer)} &= M_{n,\,NMR(Py\text{-}PPDO)} + M_{n,\,NMR(MPEG)} \\ &= 102 \times \mathrm{Dp}_{(Py\text{-}PPDO)} + 44 \\ &\quad \times \mathrm{Dp}_{(MPEG)} + 346 \end{aligned} \quad (7)$$

$$(M_{n,\,NMR(Py\text{-}PPDO)} = 102 \times \mathrm{Dp}_{(Py\text{-}PPDO)} + 231;\ M_{n,\,NMR(MPEG)} = 44 \times \mathrm{Dp}_{(MPEG)} + 115.)$$

Preparation of Micelles. The Py-$PPDO_7$-*b*-PEG_{16} copolymer was added directly to water with a concentration of 2 mg mL^{-1} at room temperature. Then an annealing treatment was performed at approximate 90 °C for a few minutes. Afterward, the system temperature was maintained at 25 °C for 24 h.

Characterization. ^{1}H NMR spectra were measured in $CDCl_3$ at 25 °C with a Bruker AV II-400 MHz spectrometer and using tetramethylsilane (TMS) as an internal standard.

Variable-temperature ^{1}H NMR spectra were measured in D_2O at different temperatures with a Bruker AV II-600 MHz spectrometer and using trimethylsilyl propionate (TSP) as an internal standard. In all measurements, temperature was maintained constant within ±0.2 °C in the range 15−80 °C, and the sample was equilibrated at the target temperature for more than 10 min prior to measurement. The concentration of samples was 6 mg mL^{-1}.

For gel permeation chromatography (GPC), the molecular weight ($M_{n,GPC}$) and the molecular weight distribution (M_w/M_n) were measured on a system equipped with a Waters 515 pump, three columns, and a 2410 differential refractometer detector. $CHCl_3$ was used as the eluent at a flow rate of 1.0 mL min^{-1} at 30 °C. Monodisperse polystyrene was used as the standard to generate the calibration curve.

The phase transition was measured by monitoring the transmittance of a 600 nm light beam through a quartz sample cell. The temperature dependence of transmittance changes was recorded on a Hitachi U-1900 spectrophotometer from 25 to 75 °C. The control of temperature was conducted by using a PolyScience temperature controller as a heating instrument. The concentration of samples was 2 mg mL^{-1}.

Fluorescence emission spectra were recorded using a Horiba Jobin Yvon FluoroMax-4 spectrofluorometer. The fixed excitation wavelength (λ_{ex}) was 341 nm. The slit widths were set at 5 nm for both excitation and emission. The control of temperature was conducted by using a PolyScience temperature controller as the heating instrument.

Bright-field transmission electron microscopy observations were performed on a Tecnai G2 F20 S-TWIN electron microscope (FEI Co.) operated at an acceleration voltage of 200 kV. The samples were prepared by depositing a drop of the aqueous suspensions of aggregates equilibrated at different temperatures or with different additives at 25 °C onto a carbon-coated copper grid. Excessive solutions were absorbed using a filter paper, and the samples were dried for several hours. All samples were stained using 2% OsO_4 solution for 10 min except for the samples containing Fe^{3+}, which were observed directly without staining.

Atomic force microscopy measurements were performed on a Digital Instrument Nanoscope IIIa multimode atomic force

microscope. The operating mode is a tapping mode under ambient conditions. The samples were prepared by spin coating the aqueous suspensions of aggregates equilibrated at different temperatures onto freshly cleaved mica surfaces.

Confocal microscopy imaging of FAMs in water was done at room temperature using a confocal laser scanning microscopy. The sample was prepared by sealing the solution between two glass plates. The concentration of the FAMs was 0.1 mg mL^{-1}.

Microcalorimetric measurements were performed on a NANO DSC (TA Instruments-Waters LLC, New Castle, DE, USA) at an external pressure of 3.0 atm using deionized water as an external reference. The cell volume was 0.33 mL. The heating rate was 1 °C min^{-1}. The testing sample with a concentration of 4.0 mg mL^{-1} in deionized water was degassed at 25 °C for 10 min and was treated as followed: First, it was kept at approximately 95 °C for 5 min and then reduced to 25 °C immediately. Finally, a certain volume of sample was placed in the NANO DSC to implement a first heating scan.

The average hydrodynamic diameter ($\langle D_h \rangle$) and size distribution of FAMs with a concentration of 2 mg mL^{-1} in water were determined at room temperature by dynamic light scattering on a Brookhaven model BI-200SM spectrometer and a 9000AT correlator using an Innova304 He−Ne laser (1 W, λ = 532 nm) at a fixed scattering angle (θ) of 90° and a correlation measurement time of 2 min with cumulant analysis and CONTIN software.

The critical micellization concentration experiments were performed as followed: a stock solution of Nile Red (4×10^{-4} mol L^{-1}) in acetone was prepared. All of the Nile Red-loaded FAMs samples were diluted with a final Nile Red concentration of 8×10^{-6} mol L^{-1}. Fluorescence emission spectra of Nile Red-loaded FAMs in deionized water with different concentrations between 2×10^{-5} and 0.1 mg mL^{-1} were obtained using a Horiba Jobin Yvon FluoroMax-4 spectrofluorometer at 25 °C. The excitation wavelength was 310 nm, and the emission range was from 590 to 700 nm. The emission and excitation slit widths were both set to 5 nm.

Conflict of Interest: The authors declare no competing financial interest.

Supporting Information Available: Synthetic routes of Py-PPDO$_7$-*b*-PEG$_{16}$. ^{1}H NMR spectra of methoxyl-PEG-COOH (MPEG-COOH), Py-PPDO-OH, and Py-PPDO-*b*-PEG. GPC traces of Py-PPDO$_7$-OH, MPEG$_{16}$-COOH, and Py-PPDO$_7$-*b*-PEG$_{16}$. Photograph of Py-PPDO$_7$-*b*-PEG$_{16}$ copolymer in $CHCl_3$ under a 365 nm UV lamp. Fluorescence emission spectra of Py-PPDO$_7$-*b*-PEG$_{16}$ in chloroform and water. Benesi−Hildebrand plot of $1/(I_0 - I)$ *versus* $1/[Fe^{3+}]$. Fluorescence emission spectra of Py-PPDO$_7$-*b*-PEG$_{16}$ in water. TEM images of FAMs. Variable-temperature ^{1}H NMR spectra of Py-PPDO$_7$-*b*-PEG$_{16}$. Nano-DSC first heating scan curve of FAMs in water. This material is available free of charge *via* the Internet at http://pubs.acs.org.

Acknowledgment. This work was financially supported by National Natural Science Foundation of China (No. 21274093 and No. 51421061). Analytical and Testing Center of Sichuan University provided NMR and TEM analysis.

REFERENCES AND NOTES

1. Du, J. Z.; O'Reilly, R. K. Anisotropic Particles with Patchy, Multicompartment and Janus Architectures: Preparation and Application. *Chem. Soc. Rev.* **2011**, *40*, 2402–2416.
2. Rahmani, S.; Lahann, J. Recent Progress with Multicompartmental Nanoparticles. *MRS Bull.* **2014**, *39*, 251–257.
3. Nisisako, T.; Torii, T.; Takahashi, T.; Takizawa, Y. Synthesis of Monodisperse Bicolored Janus Particles with Electrical Anisotropy Using a Microfluidic Co-Flow System. *Adv. Mater.* **2006**, *18*, 1152–1156.
4. Walther, A.; Matussek, K.; Müller, A. H. E. Engineering Nanostructured Polymer Blends with Controlled Nanoparticle Location Using Janus Particles. *ACS Nano* **2008**, *2*, 1167–1178.
5. Liang, F. X.; Shen, K.; Qu, X. Z.; Zhang, C. L.; Wang, Q.; Li, J. L.; Liu, J. G.; Yang, Z. Z. Inorganic Janus Nanosheets. *Angew. Chem., Int. Ed.* **2011**, *50*, 2379–2382.
6. McConnell, M. D.; Kraeutler, M. J.; Yang, S.; Composto, R. J. Patchy and Multiregion Janus Particles with Tunable Optical Properties. *Nano Lett.* **2010**, *10*, 603–0609.
7. Yoshida, M.; Roh, K. H.; Lahann, J. Short-Term Biocompatibility of Biphasic Banocolloids with Potential Use as Anisotropic Imaging Probes. *Biomaterials* **2007**, *28*, 2446–2456.
8. Lv, W.; Lee, K. J.; Li, J.; Park, T.-H.; Hwang, S.; Hart, A. J.; Zhang, F.; Lahann, J. Anisotropic Janus Catalysts for Spatially Controlled Chemical Reactions. *Small* **2012**, *8*, 3116–3122.
9. Glotzer, S. C.; Solomon, M. J. Anisotropy of Building Blocks and Their Assembly into Complex Structures. *Nat. Mater.* **2007**, *6*, 557–562.
10. Jiang, S.; Chen, Q.; Tripathy, M.; Luijten, E.; Schweizer, K. S.; Granick, S. Janus Particle Synthesis and Assembly. *Adv. Mater.* **2010**, *22*, 1060–1071.
11. Lee, K. J.; Yoon, J.; Lahann, J. Recent Advances with Anisotropic Particles. *Curr. Opin. Colloid Interface Sci.* **2011**, *16*, 195–202.
12. Hu, J.; Zhou, S. X.; Sun, Y. Y.; Fang, X. S.; Wu, L. M. Fabrication, Properties and Applications of Janus Particles. *Chem. Soc. Rev.* **2012**, *41*, 4356–4378.
13. Wang, J.-Y.; Wang, Y.; Sheiko, S. S.; Betts, D. E.; DeSimone, J. M. Tuning Multiphase Amphiphilic Rods to Direct Self-Assembly. *J. Am. Chem. Soc.* **2012**, *134*, 5801–5806.
14. Zhao, Y.; Gu, H.; Xie, Z.; Shum, H. C.; Wang, B.; Gu, Z. Bioinspired Multifunctional Janus Particles for Droplet Manipulation. *J. Am. Chem. Soc.* **2013**, *135*, 54–57.
15. Choi, C. H.; Weitz, D. A.; Lee, C. S. One Step Formation of Controllable Complex Emulsions: From Functional Particles to Simultaneous Encapsulation of Hydrophilic and Hydrophobic Agents into Desired Position. *Adv. Mater.* **2013**, *25*, 2536–2541.
16. Rahmani, S.; Saha, S.; Durmaz, H.; Donini, A.; Misra, A. C.; Yoon, J.; Lahann, J. Chemically Orthogonal Three-Patch Microparticles. *Angew. Chem., Int. Ed.* **2014**, *53*, 2332–2338.
17. Yan, X.; Su, Y.; Li, J.; Früh, J.; Möhwald, H. Uniaxially Oriented Peptide Crystals for Active Optical Waveguiding. *Angew. Chem., Int. Ed.* **2011**, *50*, 11186–11191.
18. Zou, Q.; Zhang, L.; Yan, X.; Wang, A.; Ma, G.; Li, J.; Möhwald, H.; Mann, S. Multifunctional Porous Microspheres Based on Peptide-Porphyrin Hierarchical Co-Assembly. *Angew. Chem., Int. Ed.* **2014**, *53*, 2366–2370.
19. Liu, K.; Xing, R.; Chen, C.; Shen, G.; Yan, L.; Zou, Q.; Ma, G.; Möhwald, H.; Yan, X. Peptide-Induced Hierarchical Long-Range Order and Photocatalytic Activity of Porphyrin Assemblies. *Angew. Chem., Int. Ed.* **2015**, *54*, 500–505.
20. Huang, X.; Qian, Q.; Wang, Y. Anisotropic Particles from a One-Pot Double Emulsion Induced by Partial Wetting and Their Triggered Release. *Small* **2014**, *10*, 1412–1420.
21. Walther, A.; Müller, A. H. E. Janus Particles: Synthesis, Self-Assembly, Physical Properties, and Applications. *Chem. Rev.* **2013**, *113*, 5194–5261.
22. Gädt, T.; Ieong, N. S.; Cambridge, G.; Winnik, M. A.; Manners, I. Complex and Hierarchical Micelle Architectures from Diblock Copolymers Using Living, Crystallization-Driven Polymerizations. *Nat. Mater.* **2009**, *8*, 144–150.
23. Rupar, P. A.; Chabanne, L.; Winnik, M. A.; Manners, I. Non-Centrosymmetric Cylindrical Micelles by Unidirectional Growth. *Science* **2012**, *337*, 559–562.
24. Gröschel, A. H.; Schacher, F. H.; Schmalz, H.; Borisov, O. V.; Zhulina, E. B.; Walther, A.; Müller, A. H. E. Precise Hierarchical Self-Assembly of Multicompartment Micelles. *Nat. Commun.* **2012**, *3*, 710.
25. Gröschel, A. H.; Walther, A.; Löbling, T. I.; Schacher, F. H.; Schmalz, T.; Müller, A. H. E. Guided Hierarchical Co-assembly of Soft Patchy Nanoparticles. *Nature* **2013**, *503*, 247–251.
26. Zhu, J.; Zhang, S.; Zhang, F.; Wooley, K. L.; Pochan, D. J. Hierarchical Assembly of Complex Block Copolymer Nanoparticles into Multicompartment Superstructures through Tunable Interparticle Associations. *Adv. Funct. Mater.* **2013**, *23*, 1767–1773.
27. Ding, W.; Li, Y.; Xia, H.; Wang, D.; Tao, X. Synthesis of Janus Particles *via* Strain-Driven Microphase Separation and

Their Assembly into Nanoscale Vesicles. *ACS Nano* **2014**, *8*, 11206–11213.
28. Warren, N. J.; Armes, S. P. Polymerization-Induced Self-Assembly of Block Copolymer Nano-Objects *via* RAFT Aqueous Dispersion Polymerization. *J. Am. Chem. Soc.* **2014**, *136*, 10174–10185.
29. Du, J.; Armes, S. P. Patchy Multi-Compartment Micelles are Formed by Direct Dissolution of an ABC Triblock Copolymer in Water. *Soft Matter* **2010**, *6*, 4851–4857.
30. Staff, R. H.; Gallei, M.; Mazurowski, M.; Rehahn, M.; Berger, R.; Landfester, K.; Crespy, D. Patchy Nanocapsules of Poly(vinylferrocene)-Based Block Copolymers for Redox-Responsive Release. *ACS Nano* **2012**, *6*, 9042–9049.
31. Li, Z.; Kesselman, E.; Talmon, Y.; Hillmyer, M. A.; Lodge, T. P. Multicompartment Micelles from ABC Miktoarm Stars in Water. *Science* **2004**, *306*, 98–101.
32. Kubowicz, S.; Baussard, J.-F.; Lutz, J.-F.; Thünemann, A. F.; von Berlepsch, H.; Laschewsky, A. Multicompartment Micelles Formed by Self-Assembly of Linear ABC Triblock Copolymers in Aqueous Medium. *Angew. Chem., Int. Ed.* **2005**, *44*, 5262–5265.
33. Moughton, A. O.; Hillmyer, M. A.; Lodge, T. P. Multicompartment Block Polymer Micelles. *Macromolecules* **2012**, *45*, 2–19.
34. Lin, S.; Zhu, W.; He, X.; Xing, Y.; Liang, L.; Chen, T.; Lin, J. Multicompartmental Hollow Micelles Formed by Linear ABC Triblock Copolymers in Aqueous Medium. *J. Phys. Chem. B* **2013**, *117*, 2586–2593.
35. Cui, H.; Chen, Z.; Zhong, S.; Wooley, K. L.; Pochan, D. J. Block Copolymer Assembly *via* Kinetic Control. *Science* **2007**, *317*, 647–650.
36. Nie, L.; Liu, S.; Shen, W.; Chen, D.; Jiang, M. One-Pot Synthesis of Amphiphilic Polymeric Janus Particles and Their Self-Assembly into Supermicelles with a Narrow Size Distribution. *Angew. Chem., Int. Ed.* **2007**, *46*, 6321–6324.
37. Gröschel, A. H.; Walther, A.; Löbling, T. I.; Schmelz, J.; Hanisch, A.; Schmalz, H.; Müller, A. H. Facile, Solution-Based Synthesis of Soft, Nanoscale Janus Particles with Tunable Janus Balance. *J. Am. Chem. Soc.* **2012**, *134*, 13850–13860.
38. Warren, N. J.; Mykhaylyk, O. O.; Mahmood, D.; Ryan, A. J.; Armes, S. P. RAFT Aqueous Dispersion Polymerization Yields Poly(ethylene glycol)-Based Diblock Copolymer Nano-objects with Predictable Single Phase Morphologies. *J. Am. Chem. Soc.* **2014**, *136*, 1023–1033.
39. Geng, Y.; Dalhaimer, P.; Cai, S.; Tsai, R.; Tewari, M.; Minko, T.; Discher, D. E. Shape Effects of Filaments *versus* Spherical Particles in Flow and Drug Delivery. *Nat. Nanotechnol.* **2007**, *2*, 249–255.
40. Rinkenauer, A. C.; Schallon, A.; Günther, U.; Wagner, M.; Betthausen, E.; Schubert, U. S.; Schacher, F. H. A Paradigm Change: Efficient Transfection of Human Leukemia Cells by Stimuli-Responsive Multicompartment Micelles. *ACS Nano* **2013**, *7*, 9621–9631.
41. Lodge, T. P.; Rasdal, A.; Li, Z.; Hillmyer, M. A. Simultaneous, Segregated Storage of Two Agents in a Multicompartment Micelle. *J. Am. Chem. Soc.* **2005**, *127*, 17608–17609.
42. Betthausen, G. E.; Drechsler, M.; Förtsch, M.; Schacher, F. H.; Müller, A. H. E. Dual Stimuli-Responsive Multicompartment Micelles from Triblock Terpolymers with Tunable Hydrophilicity. *Soft Matter* **2011**, *7*, 8880–8891.
43. Sun, G.; Cui, H.; Lin, L. Y.; Lee, N. S.; Yang, C.; Neumann, W. L.; Freskos, J. N.; Shieh, J. J.; Dorshow, R. B.; Wooley, K. L. Multicompartment Polymer Nanostructures with Ratiometric Dual-Emission pH-Sensitivity. *J. Am. Chem. Soc.* **2011**, *133*, 8534–8543.
44. Synatschke, C. V.; Nomoto, T.; Cabral, H.; Förtsch, M.; Toh, K.; Matsumoto, Y.; Miyazaki, K.; Hanisch, A.; Schacher, F. H.; Kishimura, A.; *et al*. Multicompartment Micelles with Adjustable Poly(ethylene glycol) Shell for Efficient *in Vivo* Photodynamic Therapy. *ACS Nano* **2014**, *8*, 1161–1172.
45. Klinger, D.; Wang, C. X.; Connal, L. A.; Audus, D. J.; Jang, S. G.; Kraemer, S.; Killops, K. L.; Fredrickson, G. H.; Kramer, E. J.; Hawker, C. J. A Facile Synthesis of Dynamic, Shape-Changing Polymer Particles. *Angew. Chem., Int. Ed.* **2014**, *53*, 7018–7022.
46. Wu, G.; Chen, S.-C.; Wang, X.-L.; Yang, K.-K.; Wang, Y.-Z. Dynamic Origin and Thermally Induced Evolution of New Self-Assembled Aggregates from an Amphiphilic Comb-like Graft Copolymer: A Multiscale and Multimorphological Procedure. *Chem.—Eur. J.* **2012**, *18*, 12237–12241.
47. Zhai, F.-Y.; Huang, W.; Wu, G.; Jing, X.-K.; Wang, M.-J.; Chen, S.-C.; Wang, Y.-Z.; Chin, I.-J.; Liu, Y. Nanofibers with Very Fine Core-Shell Morphology from Anisotropic Micelle of Amphiphilic Crystalline-Coil Block Copolymer. *ACS Nano* **2013**, *7*, 4892–4901.
48. Wang, H.; Liu, C.-L.; Wu, G.; Chen, S.-C.; Song, F.; Wang, Y.-Z. Temperature Dependent Morphological Evolution and the Formation Mechanism of Anisotropic Nano-Aggregates from a Crystalline-Coil Block Copolymer of Poly(*p*-dioxanone) and Poly(ethylene glycol). *Soft Matter* **2013**, *9*, 8712–8722.
49. Chen, S.-C.; Li, L.-L.; Wang, H.; Wu, G.; Wang, Y.-Z. Synthesis and Micellization of Amphiphilic Multi-Branched Poly(*p*-dioxanone)-*block*-poly(ethylene glycol). *Polym. Chem.* **2012**, *3*, 1231–1238.
50. Chen, S.-C.; Wu, G.; Shi, J.; Wang, Y.-Z. Novel "Star Anise"-like Nano Aggregate Prepared by Self-Assembling of Preformed Microcrystals from Branched Crystalline-Coil Alternating Multi-Block Copolymer. *Chem. Commun.* **2011**, *47*, 4198–4200.
51. Scott, A. C.; Buchanan, J. W.; Flynn, N. D.; Duncan, M. A. Photodissociation of Iron-Pyrene and Iron-Perylene Cation Complexes. *Int. J. Mass Spectrom.* **2007**, *266*, 149–155.
52. Simon, A.; Joblin, C. Thermochemistry and Infrared Spectroscopy of Neutral and Cationic Iron-Polycyclic Aromatic Hydrocarbon Complexes of Astrophysical Interest: Fundamental Density Functional Theory Studies. *J. Phys. Chem. A* **2007**, *111*, 9745–9755.
53. Winnik, F. M. Photophysics of Preassociated Pyrenes in Aqueous Polymer Solutions and in Other Organized Media. *Chem. Rev.* **1993**, *93*, 587–614.
54. Lee, E. S.; Oh, K. T.; Kim, D.; Youn, Y. S.; Bae, Y. H. Tumor pH-Responsive Flower-like Micelles of Poly(*l*-lactic acid)-*b*-poly(ethylene glycol)-*b*-poly(*l*-histidine). *J. Controlled Release* **2007**, *123*, 19–26.
55. Gai, L.; Chen, H.; Zou, B.; Lu, H.; Lai, G.; Li, Z.; Shen, Z. Ratiometric Fluorescence Chemodosimeters for Fluoride Anion Based on Pyrene Excimer/Monomer Transformation. *Chem. Commun.* **2012**, *48*, 10721–10723.
56. Dai, Q.; Liu, W.; Zhuang, X.; Wu, J.; Zhang, H.; Wang, P. Ratiometric Fluorescence Sensor Based on a Pyrene Derivative and Quantification Detection of Heparin in Aqueous Solution and Serum. *Anal. Chem.* **2011**, *83*, 6559–6564.
57. Huang, J.; Wu, Y.; Chen, Y.; Zhu, Z.; Yang, X.; Yang, C. J.; Wang, K.; Tan, W. Pyrene-Excimer Probes Based on the Hybridization Chain Reaction for the Detection of Nucleic Acids in Complex Biological Fluids. *Angew. Chem., Int. Ed.* **2011**, *50*, 401–404.
58. Conlon, P.; Yang, C. J.; Wu, Y.; Chen, Y.; Martinez, K.; Kim, Y.; Stevens, N.; Marti, A. A.; Jockusch, S.; Turro, N. J.; *et al*. Pyrene Excimer Signaling Molecular Beacons for Probing Nucleic Acids. *J. Am. Chem. Soc.* **2008**, *130*, 336–342.
59. Yang, C. J.; Jockusch, S.; Vicens, M.; Turro, N. J.; Tan, W. Light-Switching Excimer Probes for Rapid Protein Monitoring in Complex Biological Fluids. *Proc. Natl. Acad. Sci. U. S.A.* **2005**, *102*, 17278–17283.
60. Fery-Forgues, S.; Le Bris, M. T.; Guette, J. P.; Valeur, B. Ion-Responsive Fluorescent Compounds. 1. Effect of Cation Binding on Photophysical Properties of Benzoxazinone Derivative Linked to Monoaza-15-Crown-5. *J. Phys. Chem.* **1988**, *92*, 6233–6237.
61. Benesi, H. A.; Hildebrand, J. H. A Spectrophotometric Investigation of the Interaction of Iodine with Aromatic Hydrocarbons. *J. Am. Chem. Soc.* **1949**, *71*, 2703–2707.
62. Cheng, R.; Feng, F.; Meng, F. H.; Deng, C.; Feijen, J.; Zhong, Z. Y. Glutathione-Responsive Nano-Vehicles as a Promising Platform for Targeted Intracellular Drug and Gene Delivery. *J. Controlled Release* **2011**, *152*, 2–12.

63. Balendiran, G. K.; Dabur, R.; Fraser, D. The Role of Glutathione in Cancer. *Cell Biochem. Funct.* **2004**, *22*, 343–352.
64. Schafer, F. Q.; Buettner, G. R. Redox Environment of the Cell as Viewed through the Redox State of the Glutathione Disulfide/Glutathione Couple. *Free Radical Biol. Med.* **2001**, *30*, 1191–1212.
65. Deneke, S. M. Thiol-Based Antioxidants. *Curr. Top. Cell. Regul.* **2000**, *36*, 151–180.
66. Liu, J.; Huang, W.; Pang, Y.; Huang, P.; Zhu, X.; Zhou, Y.; Yue, D. Molecular Self-Assembly of a Homopolymer: An Alternative to Fabricate Drug-Delivery Platforms for Cancer Therapy. *Angew. Chem., Int. Ed.* **2011**, *50*, 9162–9166.
67. Klaikherd, A.; Nagamani, C.; Thayumanavan, S. Multi-Stimuli Sensitive Amphiphilic Block Copolymer Assemblies. *J. Am. Chem. Soc.* **2009**, *131*, 4830–4838.
68. Zhao, F.; Shen, G.; Chen, C.; Xing, R.; Zou, Q.; Ma, G.; Yan, X. Nanoengineering of Stimuli-Responsive Protein-Based Biomimetic Protocells as Versatile Drug Delivery Tools. *Chem.—Eur. J.* **2014**, *20*, 6880–6887.
69. Nakahata, M.; Takashima, Y.; Yamaguchi, H.; Harada, A. Redox-Responsive Self-Healing Materials Formed from Host-Guest Polymers. *Nat. Commun.* **2011**, *2*, 511.
70. Netto, L. E.; Stadtman, E. R. The Iron-Catalyzed Oxidation of Dithiothreitol Is a Biphasic Process: Hydrogen Peroxide Is Involved in the Initiation of a Free Radical Chain of Reactions. *Arch. Biochem. Biophys.* **1996**, *333*, 233–242.
71. Cheng, L.; Zhang, G.; Zhu, L.; Chen, D.; Jiang, M. Nanoscale Tubular and Sheetlike Superstructures from Hierarchical Self-Assembly of Polymeric Janus Particles. *Angew. Chem., Int. Ed.* **2008**, *47*, 10171–10174.
72. Wu, G.; Chen, S.-C.; Zhan, Q.; Wang, Y.-Z. Well-Defined Amphiphilic Biodegradable Comb-Like Graft Copolymers: Their Unique Architecture-Determined LCST and UCST Thermoresponsivity. *Macromolecules* **2011**, *44*, 999–1008.
73. Israelachvili, J. The Different Faces of Poly(ethylene glycol). *Proc. Natl. Acad. Sci. U.S.A.* **1997**, *94*, 8378–8379.